ACS Medicinal Chemistry Letters

Letter

pubs.acs.org/acsmedchemlett

Vivid Tumor Imaging Utilizing Liposome-Carried Bimodal Radiotracer

Jonghee Kim,[†] Darpan N. Pandya,[†] Woonghee Lee,[†] Jang Woo Park,[‡] Youn Ji Kim,[†] Wonjung Kwak,[†] Yeong Su Ha,[†] Yongmin Chang,[†,‡] Gwang Il An,*[,§] and Jeongsoo Yoo*[,†]

[†]Department of Molecular Medicine, BK21 Plus KNU Biomedical Convergence Program, Kyungpook National University, Daegu 700-422, South Korea

[‡]Department of Medical & Biological Engineering, Kyungpook National University, Daegu 700-422, South Korea

[§]Molecular Imaging Research Center, KIRAMS, Seoul 139-706, South Korea

Supporting Information

ABSTRACT: By developing a new bimodal radioactive tracer that emits both luminescence and nuclear signals, a trimodal liposome for optical, nuclear, and magnetic resonance imaging is efficiently prepared. Fast clearance of the radiotracer from reticuloendothelial systems enables vivid tumor imaging with minimum background.

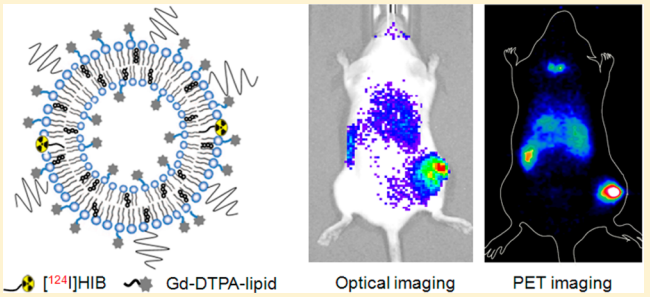

KEYWORDS: *Imaging agent, radiopharmaceutical, multimodal imaging, Cerenkov radiation, liposome*

It is now well accepted that multimodal imaging is more efficient and accurate in the diagnosis of various diseases.[1,2] Along with the development of multimodal imaging instruments (e.g., PET (positron emission tomography)/CT (computed tomography), SPECT (single photon emission computed tomography)/CT, PET/MR (magnetic resonance), optical/PET, optical/MR scanner),[3] a variety of multimodal imaging probes have been synthesized and tested as new contrasting agents.[4,5] Among several multimodal imaging platforms, metal-based nanocrystals such as iron oxide, quantum dots, and gold nanoparticles have been especially preferred because these nanocrystals can serve as intrinsic MR, optical, and CT contrasting agents, respectively, and only additional imaging components are needed.[6,7] However, after systemic injection, many nanocrystal-based imaging agents showed slow clearance from the reticuloendothelial system (RES, e.g., liver and spleen), and toxicity and safety issues remain as a substantial hurdle for further advancement to clinical applications, especially when radiolabeled for nuclear imaging.[8,9] The radiolabeled imaging agent should be excreted within certain time period from nontarget organs to minimize unnecessary radiation exposures. Furthermore, the slow clearance increases background noise to make accurate tumor detection difficult in nuclear imaging.

In contrast, liposomes are the more preferred option to develop multimodal imaging probes for clinical application as it is made up from biocompatible, nontoxic, and biodegradable materials.[10,11] Many liposomes are already FDA approved for effective drug delivery carriers.[12] Furthermore, liposomes have many attractive characteristics as a multimodal imaging platform, including a well-established preparation method, easy size control, easy surface modification, large loading capacity, and excellent in vivo stability.[13] The only drawback is that all imaging contrast components should be added into liposomes to become multimodal imaging probe.[5] However, as the number of different imaging contrast components is increased, the liposome preparation process becomes complicated, and various issues regarding characterization and reproducibility are raised. Probably, this is why very few liposome-based trimodality imaging probes have been reported so far.[14,15]

Here we report on a new strategy for preparation of a trimodal liposome for optical, nuclear, and MR tumor imaging. By synthesizing a new radioactive tracer emitting luminescent light, hybrid trimodal liposomes were prepared by supplementing with only two different imaging components instead of three. The radiotracer excreted fast from RES resulting in vivid tumor imaging with high tumor-to-background ratio.

First, we developed a new radioactive tracer capable of emitting both nuclear and optical imaging signals. Recently, Cerenkov radiation, which is the light emitted when a charged particle travels with a velocity greater than that of light in a given medium, seeks new application in optical molecular imaging.[16,17] We screened Cerenkov luminescence properties

Received: December 13, 2013
Accepted: February 4, 2014
Published: February 4, 2014

   dx.doi.org/10.1021/ml400513g | ACS Med. Chem. Lett. 2014, 5, 390−394

of various radionuclides and found that some radionuclides commonly used for PET imaging such as ^{68}Ga, ^{124}I, ^{18}F, and ^{64}Cu emit strong Cerenkov light.[18,19]

Among these radionuclides, ^{124}I was chosen as a radioisotope source because of its attractive physical properties; long half-life (4.2 d), which allows sufficient time for preparation and for ease of conducting long follow-up studies after administration, and the high kinetic energy of positrons emitted during decay ($E_{\beta+}$ mean, 819 keV) leading to strong Cerenkov luminescence light (2.5 and 6 times stronger compared to ^{18}F and ^{64}Cu, respectively).[19]

For efficient incorporation into the liposomal bilayer and high in vivo stability of radio-iodinated compounds, a long alkyl chain linked with a 4-iodobenzoyl group was designed as a target compound (Figure 1a). The lipophilic long alkyl chains

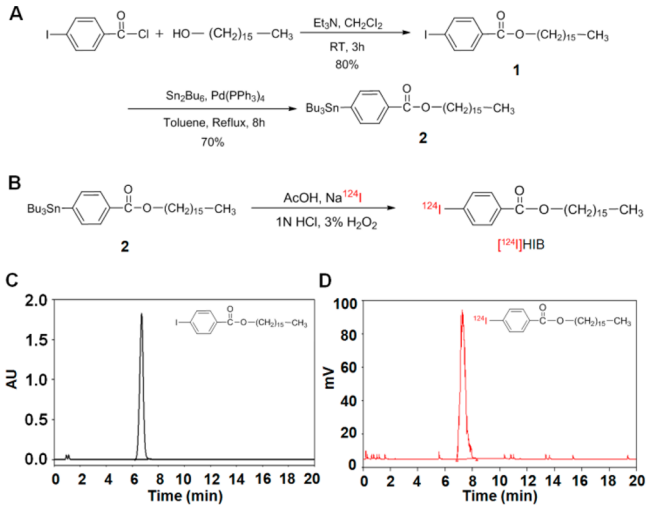

Figure 1. Synthesis scheme of standard and precursor for HIB (a), radiolabeling scheme of [^{124}I]HIB (b), UV chromatogram of HIB (c), and radio chromatogram of [^{124}I]HIB (d).

were widely used for tight anchor on cell membrane,[20] and iodo-aryl compound was selected to minimize deiodination in physiological conditions.[21] Nonradioactive standard hexadecyl-4-iodo benzoate (1, HIB) was prepared by esterification of 4-iodobenzoyl chloride with 1-hexadecanol in the presence of triethylamine as a base. The crude product was extracted with dichloromethane and recrystallized to give white crystalline needles (80% yield). For the preparation of precursor for radiolabeling, to a solution of hexadecyl-4-iodobenzoate dissolved in toluene, hexabutylditin and a catalytic amount of $Pd(Ph_3)_4$ were added, refluxed, concentrated, and purified by column chromatography to afford pure hexadecyl-4-tributyl-stannylbenzoate (2) in 71% yield.

For radio-iodination, the tributylstannyl group of 2 was replaced by radioactive iodine-124 (Figure 1b). The precursor 2 was reacted with [^{124}I]NaI (0.5−5 mCi) in the presence of acetic acid and 3% H_2O_2. The mixture was shaken for 30 min at 70 °C and dried completely under vacuum. Only radiolabeled hexadecyl-4-[^{124}I]iodobenzoate ([^{124}I]HIB) was simply extracted by acetonitrile, concentrated, and reconstituted in dichloromethane for the following studies. Its radiochemical yield was over 90%, and the radiochemical purity reached 100% after the extraction, as determined by radio-TLC and radio-HPLC analysis [Luna C8 column, 4.6 × 50 mm, 5 μm; 95:5 MeCN/H_2O, 1 mL/min flow rate] (Figure 1c,d). All radiolabeling and purification steps were finished less than 40 min without any time-consuming HPLC purification.

A trimodal liposome was prepared by one-pot formulation of phosphatidylcholine, cholesterol, PEGylated lipid, lipophilic gadolinium complex, and the radiolabeled [^{124}I]HIB (Figure 2).

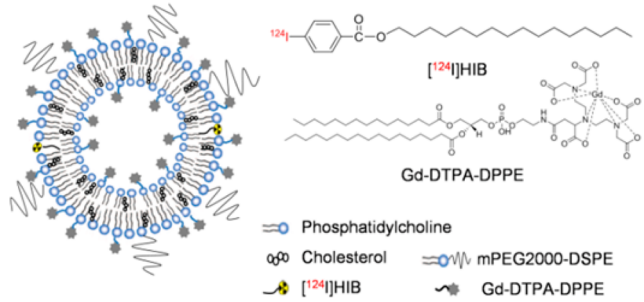

Figure 2. Schematic diagram of trimodal liposome and its imaging components.

A chloroform solution of 1,2-dipalmitoyl-*sn*-glycero-3-phospho choline (DPPC), 1,2-dihexadecanoyl-*sn*-glycero-3-phospho-(1′-rac-glycerol) (DPPG), cholesterol, 1,2-distearoyl-*sn*-glycero-3-phosphoethanolamine-*N*[methoxy(polyethylene glycol)-2000] (DSPE-PEG2000), and gadolinium-1,2-dipalmitoyl-*sn*-glycero-3-phosphoethanolamine-*N*-diethylenetriaminepenta acetic acid (Gd-DTPA-DPPE) at a molar ratio of 8:8:3:1:7 and [^{124}I]HIB were well mixed and dried to form a thin lipid film, which was hydrated with saline for 25 min at 50 °C.[22,23] The resultant opaque liposomal solution was sequentially extruded through membrane filters with a pore size of 1000, 400, 200, and 100 nm. The extruded liposome was further purified using a size exclusion column (PD-10, GE Healthcare).

The formed liposome was characterized using a dynamic light scattering (DLS) size analyzer and transmission electron microscopy (TEM). In DLS measurements, the liposomes showed good size distribution of mean diameter of 127.8 ± 8.4 nm (Figure 3a). Negative staining TEM images also confirmed globular liposomal structure of ca. 120 nm (Figure 3b). The lipid bilayer was clearly identifiable in TEM imaging. The PEGylated lipid (DSPE-PEG2000) was added as one of the liposome components in order to reduce the immediate capture of liposomes by the RES after systemic administration and to allow longer blood circulation time for higher tumor accumulation.[24] The liposome diameter of ca. 100 nm was chosen in order to maximize passive tumor targeting due to enhanced permeability and retention effect.[25]

Each 200 μL fraction of the prepared radioactive liposome from the size exclusion column was collected and counted using a gamma counter. Most radiolabeled liposomes were eluted at an elution volume of around 4 mL (Figure 3c), while the free [^{124}I]HIB was stuck to the column because of its extremely low water solubility (log P = 2.19 ± 0.04). The radio-incorporation yield of [^{124}I]HIB into liposome was over 75% after column purification. All eluted fractions were transferred to a 96-well plate and imaged by luminescence and PET and MR imaging (Figure 3d). As expected, the optical luminescence imaging pattern matched well with that of PET imaging because both optical and nuclear imaging signals originate from the radioactive [^{124}I]HIB. However, upon close examination, the optical imaging showed better spatial resolution and higher sensitivity than nuclear PET imaging.[18,26] When considering much shorter imaging time of optical imaging compared to

dx.doi.org/10.1021/ml400513g | ACS Med. Chem. Lett. 2014, 5, 390−394

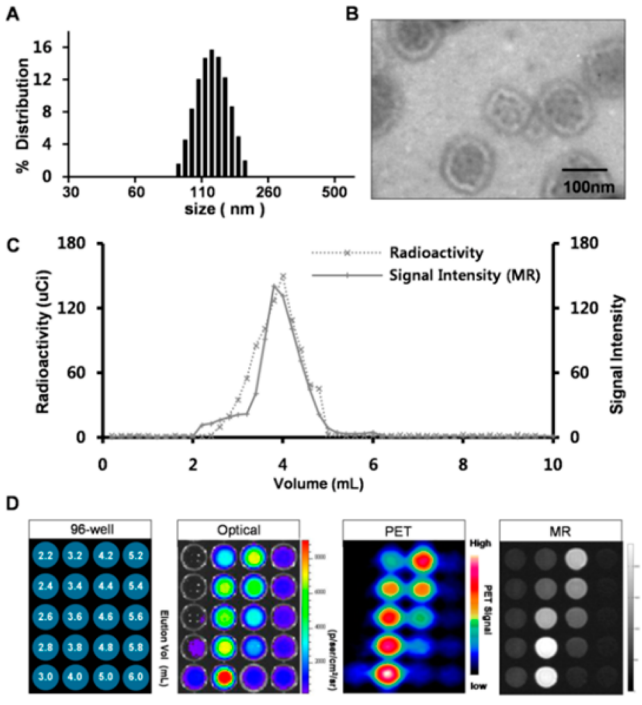

Figure 3. Size distribution of liposome measured by DLS analyzer (a), TEM image of liposome (b), size exclusion chromatogram profile of [^{124}I]HIB-Gd-containing liposome (c), and optical, PET, and MR images of SEC elution fractions (d).

nuclear imaging (1 min vs 20 min, respectively), it becomes more obvious that optical imaging is a better choice for ex vivo characterization than nuclear imaging. MR imaging of the same well plate showed a precise outline of each well because of its excellent spatial resolution. The MR signal intensity of each well was closely related to the well's radioactivity (Figure 3d), indicating that both [^{124}I]HIB and the Gd-DTPA complex were well incorporated into the liposome and move together. However, even though a 5×10^4-fold excess of Gd complexes (2.4×10^{-7} mol in 200 μL well at 4 mL elution point, ICP measurement) was contained within the same liposome in comparison to [^{124}I]HIB (4.8×10^{-12} mol, equivalent to 150 μCi), because of its poor sensitivity, fewer wells were differentiated from the adjacent background wells in MR imaging compared with optical and PET imaging. An extremely large loading capacity of liposomes made it possible to incorporate two different imaging components having such a big concentration difference into a single probe.

To characterize in vivo stability of the prepared liposomes, first, the blood half-life of [^{124}I]HIB-assembled liposome was measured by serial retro-orbital bleeds and compared to that of [^{124}I]HIB itself (n = 2 mice per group). Both blood half-life data of [^{124}I]HIB and [^{124}I]HIB-labeled liposomes fit a two-phase exponential decay model with the values of 1.3 and 70.8 min, respectively (Figure 4a,b). These huge differences of blood half-life data clearly indicated that the [^{124}I]HIB-labeled liposomes move together in the body without immediate dissociation of [^{124}I]HIB from the liposome.

Then, the purified [^{124}I]HIB-Gd-containing liposomes (150 μCi) were injected into CT26 tumor-bearing BALB/c mice for in vivo imaging studies. Because of its excellent sensitivity and short imaging time, the tumor uptake of the injected liposomes was initially monitored by optical imaging up to 48 h. With the help of photographic images of mice, the CT26 tumor was

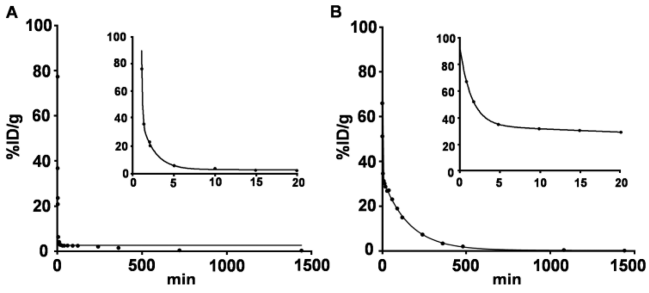

Figure 4. Blood half-life of [^{124}I]HIB (a) and [^{124}I]HIB-Gd-liposome (b) up to 24 h (n = 2). The insets show a pattern of early blood clearance (0–20 min).

most vividly imaged with minimum background at 4 h postinjection (Figure 5a-left). In addition to high uptake in

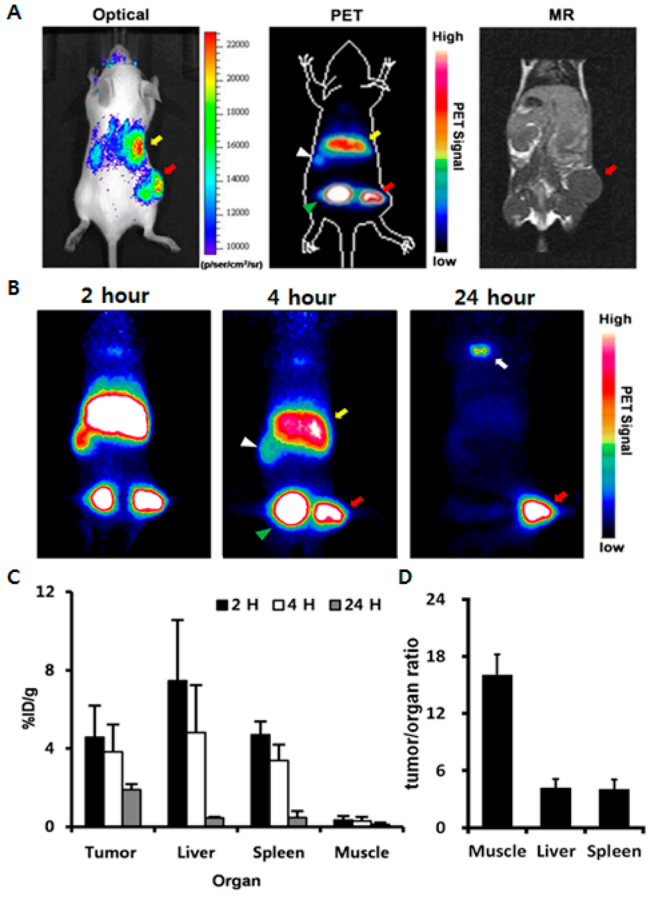

Figure 5. Typical optical luminescence, PET and MR image of CT26 tumor-bearing mouse at 4 h postinjection of [^{124}I]HIB-Gd-liposome (n = 3) (a). Tumor, red arrow; liver, yellow arrow; spleen, white arrowhead; bladder, green arrowhead. Maximum intensity projection images of PET at 2, 4, and 24 h (b). Thyroid: white arrow. Radioactivity uptakes in various organs at 2, 4, and 24 h (n = 3) (c). Tumor-to-organ uptake ratio at 24 h (d).

the tumor, other hot spots were observed around the abdominal region, which could be attributed to liver even though precise assignment was not feasible because of the poor tissue penetration and high scattering characteristics of Cerenkov light. The precise internal distribution of the liposome-carried [^{124}I]HIB was confirmed by nuclear PET imaging thanks to its high tissue penetration feature (Figure 5a-

dx.doi.org/10.1021/ml400513g | ACS Med. Chem. Lett. 2014, 5, 390–394

middle). The abdominal hot spots in optical imaging were clearly assigned as liver and spleen in tomographic PET images. PET imaging also revealed another hot spot in the bladder, which was not observed in optical image at all, presumably because of the deep location of bladder from the imaging surface in supine position. The high activity in urine could be explained by the renal excretion of catabolized [^{124}I]HIB molecules in the liver.[27] Neither liposomes of >100 nm size nor lipophilic compounds favor renal excretion.[28,29] MR imaging provided excellent anatomical information, especially regarding soft tissues, which was missing from both optical and nuclear imaging (Figure 5a-right). The tumor showed slightly enhanced contrast due to the Gd(III) complexes incorporated into the liposome (see Supporting Information). Rapid increase of contrast-to-noise ratio (CNR) was observed up to 30 min and slowly increased to maximum value at 3 h in both liver and tumor. However, the CNR values in liver and tumor were gradually decreased afterward. However, because of low sensitivity of MR imaging, the MR contrasting effect was weaker compared to optical and nuclear PET imaging.[30]

Whole body distribution and clearance pattern of the liposome-carried [^{124}I]HIB was serially monitored by PET imaging (n = 3) (Figure 5b). Most activities were accumulated in RES (liver and spleen) organs and tumor within 2 h. However, liver and spleen activities continued to decrease, while the substantial amount of activity remained in tumor up to 24 h. Interestingly, high activities were found in bladder, indicating that lipophilic [^{124}I]HIB seemed to be catabolized in liver and the hydrophilic components, presumably free [^{124}I]iodide ions and others, were cleared out by renal excretion. This hypothesis was further supported by the focal uptake of free [^{124}I]iodide in thyroid at 24 h.[21]

The radioactivities in the liver, spleen, tumor, and muscle were quantified based on PET imaging (n = 3) (Figure 5c). The highest uptake was observed in liver at 2 h, followed by tumor and spleen (7.5 ± 3.1, 4.6 ± 1.6, and 4.7 ± 0.7 %ID/g, respectively). Activities in liver and spleen continued to decrease up to 24 h, and less than 10% of 2 h activities were found at 24 h (0.45 ± 0.04 and 0.47 ± 0.3 %ID/g, respectively). However, tumor showed a much slower clearance pattern. More than 40% activity of the 2 h time point was still observed in tumor at 24 h (1.9 ± 0.29%ID/g). At 24 h, the tumor-to-muscle, tumor-to-liver, and tumor-to-spleen ratios were 16.1, 4.1, and 4.0, respectively (Figure 5d). Only tumor was clearly visualized with minimum background at 24 h. The muscle activity at 24 h is as low as 0.12 ± 0.11 %ID/g.

In conclusion, here we reported a facile method for preparation of a trimodal tumor imaging agent using liposome platform. By the development of a radiotracer that emits strong Cerenkov luminescence light, optical and nuclear images were obtained from the single imaging component. Tumors were detected by all optical, nuclear, and MR imaging modalities. The liposome-carried radiotracer showed longer retention in tumor but cleared quickly from RES organs, resulting in vivid tumor imaging with minimum background.

■ ASSOCIATED CONTENT

Supporting Information

Synthesis of HIB standard and precursor, radiolabeling, liposome preparation, in vitro and in vivo imaging studies, blood half-life measurement, and MR image analyses. This material is available free of charge via the Internet at http://pubs.acs.org.

■ AUTHOR INFORMATION

Corresponding Authors

*(J.Y.) Fax: (+82) 53-426-4944. E-mail: yooj@knu.ac.kr.
*(G.I.A.) Fax: (+82) 2-970-2409. E-mail: gwangil@kirams.re.kr.

Author Contributions

The manuscript was written through contributions of all authors. All authors have given approval to the final version of the manuscript.

Funding

This research was supported by Kyungpook National University Research Fund, 2011.

Notes

The authors declare no competing financial interest.

■ REFERENCES

(1) Swierczewska, M.; Lee, S.; Chen, X. Inorganic nanoparticles for multimodal molecular imaging. *Mol. Imaging* **2011**, *10*, 3−16.
(2) Huang, W.-Y.; Davis, J. J. Multimodality and nanoparticles in medical imaging. *Dalton Trans.* **2011**, *40*, 6087−6103.
(3) Cherry, S. R.; Semin. Multimodality imaging: beyond PET/CT and SPECT/CT. *Semin. Nucl. Med.* **2009**, *39*, 348−353.
(4) Louie, A. Multimodality Imaging Probes: Design and Challenges. *Chem. Rev.* **2010**, *110*, 3146−3195.
(5) Jarzyna, P. A.; Gianella, A.; Skajaa, T.; Knudsen, G.; Deddens, L. H.; Cormode, D. P.; Fayad, Z. A.; Mulder, W. J. M. Multifunctional imaging nanoprobes. *Wiley Interdiscip. Rev.: Nanomed. Nanobiotechnol.* **2010**, *2*, 138−150.
(6) Xie, J.; Liu, G.; Eden, H. S.; Ai, H.; Chen, X. Surface-engineered magnetic nanoparticle platforms for cancer imaging and therapy. *Acc. Chem. Res.* **2011**, *44*, 883−892.
(7) Gao, J.; Gu, H.; Xu, B. Multifunctional magnetic nanoparticles: Design, synthesis, and biomedical applications. *Acc. Chem. Res.* **2009**, *42*, 1097−1107.
(8) Krug, H. F.; Wick, P. Nanotoxicology: An interdisciplinary challenge. *Angew. Chem., Int. Ed.* **2011**, *50*, 1260−1278.
(9) Landsiedel, R.; Ma-Hock, L.; Kroll, A.; Hahn, D.; Schnekenburger, J.; Wiench, K.; Wohlleben, W. Testing metal-oxide nanomaterials for human safety. *Adv. Mater.* **2010**, *22*, 2601−2627.
(10) Kluza, E.; Jacobs, I.; Hectors, S. J. C. G.; Mayo, K. H.; Griffioen, A. W; Strijkers, G. J.; Nicolay, K. Dual-targeting of $\alpha_v\beta_3$ and galectin-1 improves the specificity of paramagnetic/fluorescent liposomes to tumor endothelium in vivo. *J. Controlled Release* **2012**, *158*, 207−214.
(11) Chow, T.-H.; Lin, Y.-Y.; Hwang, J.-J.; Wang, H.-E.; Tseng, Y.-L.; Pang, V. F.; Liu, R.-S.; Lin, W.-J.; Yang, C.-S.; Ting, G. Therapeutic efficacy evaluation of ^{111}In-labeled PEGylated liposomal vinorelbine in murine colon carcinoma with multimodalities of molecular imaging. *J. Nucl. Med.* **2009**, *50*, 2073−2081.
(12) Torchilin, V. P. Recent advances with liposomes as pharmaceutical carriers. *Nat. Rev. Drug Discovery* **2005**, *4*, 145−160.
(13) Mulder, W. J. M.; Strijkers, G. J.; van, T. G. A. F.; Cormode, D. P.; Fayad, Z. A.; Nicolay, K. Nanoparticulate assemblies of amphiphiles and diagnostically active materials for multimodality imaging. *Acc. Chem. Res.* **2009**, *42*, 904−914.
(14) Li, S.; Goins, B.; Zhang, L.; Bao, A. Novel multifunctional theranostic liposome drug delivery system: Construction, characterization, and multimodality MR, near-infrared fluorescent, and nuclear imaging. *Bioconjugate Chem.* **2012**, *23*, 1322−1332.
(15) Mitchell, N.; Kalber, T. L.; Cooper, M. S.; Sunassee, K.; Chalker, S. L; Shaw, K. P.; Ordidge, K. L.; Badar, A.; Janes, S. M.; Blower, P. J.; Lythgoe, M. F.; Hailes, H. C.; Tabor, A. B. Incorporation of paramagnetic, fluorescent and PET/SPECT contrast agents into liposomes for multimodal imaging. *Biomaterials* **2013**, *34*, 1179−1192.
(16) Robertson, R.; Germanos, M. S.; Li, C.; Mitchell, G. S.; Cherry, S. R.; Silva, M. D. Optical imaging of Cerenkov light generation from positron-emitting radiotracers. *Phys. Med. Biol.* **2009**, *54*, N355−N365.

(17) Ruggiero, A.; Holland, J. P.; Lewis, J. S.; Grimm, J. Cerenkov luminescence imaging of medical isotopes. *J. Nucl. Med.* **2010**, *51*, 1123−1130.
(18) Park, J. C.; Yu, M. K.; An, G. I.; Park, S. I.; Oh, J.; Kim, H. J.; Kim, J. H.; Wang, E. K.; Hong, I. H.; Ha, Y. S.; Choi, T. H.; Jeong, K. S.; Chang, Y.; Welch, M. J.; Jon, S.; Yoo, J. Facile preparation of a hybrid nanoprobe for triple-modality optical/PET/MR imaging. *Small* **2010**, *6*, 2863−2868.
(19) Park, J. C.; An, G. I.; Park, S.-I.; Oh, J.; Kim, H. J.; Ha, Y. S.; Wang, E. K.; Kim, K. M.; Kim, J. Y.; Lee, J.; Welch, M. J.; Yoo, J. Luminescence imaging using radionuclides: a potential application in molecular imaging. *Nucl. Med. Biol.* **2011**, *38*, 321−329.
(20) Kawamura, R.; Mishima, M.; Ryu, S.; Arai, Y.; Okose, M.; Silberberg, Y. R.; Rao, S. R.; Nakamura, C. Controlled cell adhesion using a biocompatible anchor for membrane-conjugated bovine serum albumin/bovine serum albumin mixed layer. *Langmuir* **2013**, *29*, 6429−6433.
(21) Israel, I.; Brandau, W.; Farmakis, G.; Samnick, S. Improved synthesis of no-carrier-added *p*-[^{124}I]iodo-L-phenylalanine and *p*-[^{131}I]iodo-L-phenylalanine for nuclear medicine applications in malignant gliomas. *Appl. Radiat. Isot.* **2008**, *66*, 513−522.
(22) Hadjidemetriou, M.; Pippa, N.; Pispas, S.; Demetzos, C. Incorporation of dimethoxycurcumin into charged liposomes and the formation kinetics of fractal aggregates of uncharged vectors. *J. Liposome Res.* **2013**, *23*, 94−100.
(23) Rauchhaus, U.; Schwaiger, F. W.; Panzner, S. Separating therapeutic efficacy from glucocorticoid side-effects in rodent arthritis using novel, liposomal delivery of dexamethasone phosphate: long-term suppression of arthritis facilitates interval treatment. *Arthritis Res. Ther.* **2009**, *11*, R190.
(24) Barreto, J. A.; O'Malley, W.; Kubeil, M.; Graham, B.; Stephan, H.; Spiccia, L. Nanomaterials: applications in cancer imaging and therapy. *Adv. Mater.* **2011**, *23*, H18−H40.
(25) Liu, D.; Mori, A.; Huang, L. Role of liposome size and RES blockade in controlling biodistribution and tumor uptake of GM1-containing liposomes. *Acta Biomembr.* **1992**, *1104*, 95−101.
(26) Choi, J.-S.; Park, J. C.; Nah, H.; Woo, S.; Oh, J.; Kim, K. M.; Cheon, G. J.; Chang, Y.; Yoo, J.; Cheon, J. A hybrid nanoparticle probe for dual-modality positron emission tomography and magnetic resonance imaging. *Angew. Chem., Int. Ed.* **2008**, *47*, 6259−6262.
(27) Zamboni, W. C.; Eiseman, J. L.; Strychor, S.; Rice, P. M.; Joseph, E.; Zamboni, B. A.; Donnelly, M. K.; Shurer, J.; Parise, R. A.; Tonda, M. E.; Yu, N. Y.; Basse, P. H. Tumor disposition of pegylated liposomal CKD-602 and the reticuloendothelial system in preclinical tumor models. *J. Liposome Res.* **2011**, *21*, 70−80.
(28) Wong, A. W.; Ormsby, E.; Zhang, H.; Seo, J. W.; Mahakian, L. M.; Caskey, C. F.; Ferrara, K. W. A comparison of image contrast with (64)Cu-labeled long circulating liposomes and (18)F-FDG in a murine model of mammary carcinoma. *Am. J. Nucl. Med. Mol. Imaging* **2013**, *3*, 32−43.
(29) Yoo, J.; David, E. R.; Kim, J.; Anderson, C. J.; Welch, M. J. A potential Dubin−Johnson syndrome imaging agent: synthesis, biodistribution, and microPET imaging. *Mol. Imaging* **2005**, *4*, 18−29.
(30) Gore, J. C.; Yankeelov, T. E.; Peterson, T. E.; Avison, M. J. Molecular imaging without radiopharmaceuticals? *J. Nucl. Med.* **2009**, *50*, 999−1007.